Eur. Phys. J B **18**, 233–240 (2000)

THE EUROPEAN PHYSICAL JOURNAL B

EDP Sciences

Chromium doped manganites: evidence for electronically phase-separated systems

O. Toulemonde[1,a,c], F. Studer[1], A. Barnabé[1,b], B. Raveau[1], and J.B. Goedkoop[2,c]

[1] Laboratoire CRISMAT, Université de Caen[d], ISMRA, boulevard Maréchal Juin, 14050 Caen Cedex, France
[2] ESRF, BP 220, 38043 Grenoble Cedex, France

Received 7 January 2000

Abstract. X-ray absorption spectroscopy (XAS) and soft-X-ray magnetic circular dichroism (SXMCD) at the Mn $L_{2,3}$-, Cr $L_{2,3}$- and O-K edges of $Sm_{0.5}Ca_{0.5}Mn_{1-x}Cr_xO_3$ ($0.05 \leq x \leq 0.12$) bulk polycrystalline samples have been performed at $T = 20$ K below the ferromagnetic Curie temperature. We show the existence of a magnetic sublattice on each of the probed cations. Considering an electronically phase-separated system, results are compared with magnetization and resistivity measurements and a tentative correlation with magnetoresistance properties on such doped compounds is discussed.

PACS. 75.30.Vn Colossal magnetoresistance – 78.70.Dm X-ray absorption spectra – 75.25.+z Spin arrangements in magnetically ordered materials (including neutron and spin-polarized electron studies, synchrotron-source x-ray scattering, etc.)

1 Introduction

Manganese oxide perovskites $Ln_{1-x}A_xMnO_3$ (Ln = Re; A = Ca, Sr or Ba) are at the centre of attention since the discovery of the colossal magnetoresistance at temperature close to room temperature [1].

From a fundamental point of view, the CMR effect seems to originate from a double exchange (DE) mechanism between Mn(III) and Mn(IV) species [2]. Besides, theoretical works made by Millis and co-workers [3] suggest that Jahn-Teller type electron-phonon interactions are involved in the appearance of such properties. Neutron powder diffraction studies of these manganites showing lattice evolution and variation of isotropic Debye-Waller factors at T_c [4], EXAFS (Extended X-ray Absorption Fine Structure) studies showing changes in the Debye-Waller factor at T_c [5] and XAS studies at the O K- [6] and Mn $L_{2,3}$-edges [7] showing changes in the fine structure at T_c which are interpreted as a decrease of the Jahn-Teller distortion at the metal-insulator transition, support this polaron model in addition to double-exchange physics.

Up to now, from a phase segregation point of view [8], the magnetoresistance phenomenon seems to be the same for all manganites $Ln_{1-x}A_xMnO_3$ even if two types of behavior based on the thermal variations of resistance without applied magnetic field can be distinguished. The type I manganites exhibit an insulator to metal transition (IM) with decreasing temperature whereas type II manganites exhibit a semi-conducting behavior down to 4.2 K due to the existence of charge ordering (CO) phenomena. Moreover, the magnetic ordering in these type II manganites is limited to a short range ferromagnetic coupling down to T_N, temperature at which a long-range antiferromagnetic ordering occurs at lower temperatures. However, an insulator-metal transition can again be induced in the latter phases by doping the Mn sites with transition metal elements such as cobalt, nickel or chromium [9].

Preliminary XAS studies at Cr, Co, Ni and Mn K-edges showed that the formal charges of the doping elements are Ni^{2+}, Co^{2+} and Cr^{3+} [10]. The existence and orientation of a magnetic moment on the doping transition metals (TM) is of importance to understand the nature of magnetic interactions in the doped manganites and hence their influence on the electron transport properties.

Here, we present detailed X-ray absorption spectroscopy data at low temperature of Mn $L_{2,3}$-, Cr $L_{2,3}$- and O-K edges and a soft X-ray magnetic circular dichroim study at the Mn $L_{2,3}$-, Cr $L_{2,3}$-and O K-edges of $Sm_{0.5}Ca_{0.5}Mn_{1-x}Cr_xO_3$ ($0.05 \leq x \leq 0.12$) series. Specifically, the relative orientation of the magnetic moments is determined for the probed cations and results

[a] e-mail: toulemon@wins.uva.nl
[b] *Present address*: Laboratoire L.C.M.I./C.I.R.I.Mat. CNRS UMR 5085 - Université Paul Sabatier, Toulouse III, 31062 Toulouse Cedex 4, France
[c] *Present address*: Faculty of Mathematics, Computer Science, Physics and Astronomy, University of Amsterdam, Valckenierstraat 65, 1018 XE Amsterdam, The NetherLands
[d] UMR 6508 associée au CNRS

are compared with the corresponding magnetization and electron transport properties considering an electronically phase-separated system.

2 Experimental

The rare earth manganites $Sm_{0.5}Ca_{0.5}Mn_{1-x}Cr_xO_3$ ($0.05 \leq x \leq 0.12$) were prepared in the form of sintered pellets following a classical method of solid state chemistry. Thorough mixtures of oxides CaO, Mn_2O_3, Sm_2O_3 and Cr_2O_3 were first heated in air at 950 °C for 12 hours. The samples were then pressed into pellets and sintered first at 1 200 °C and then at 1 500 °C for 12 hours in air. X-ray powder diffraction measurement showed single phase patterns.

Magnetization curves $M(T)$ were established with a vibrating sample magnetometer. Samples were first zero-field cooled to 5 K before the magnetic field was applied. Measurements were carried out under warming. Resistance measurements were performed with the four probe technique on sintered bars with $2\times2\times10$ mm^3 dimensions. Magnetoresistance measurements were performed with a quantum design physicals properties measurements systems (PPMS). Resistance was measured with increasing temperature under 0.55 T.

The X-ray magnetic circular dichroism and X-ray absorption studies of these phases were performed systematically on the samples previously studied for their transport and magnetic properties by electron diffraction and microscopy [11].

X-ray absorption spectra at Mn, Cr $L_{2,3}$-edges and O K-edges were recorded using circular polarized light at the Dragon beamline (ID 12B) of the ESRF (Grenoble, France). To remove residual asymmetries, XAS and XMCD spectra were obtained by measuring the total yield signal at each photon energy for fields of plus or minus 0.55 tesla, both helicities were used with polarization between 80 and 90% (± 5%) measured between 700 and 900 eV [12]. The base pressure in the spectrometer chamber was better than 10^{-9} mbar when the samples were scraped just before measurement and it was maintained below this value during the measurement time. All the SXMCD spectra were taken at 20 K below the ferromagnetic Curie temperature of the samples. The SXMCD signals were corrected for partial circular polarization and are normalized to L_3-edge after background removal following a procedure described by Chen *et al.* [13].

X-ray absorption spectra at O K-edges were recorded using linear polarized light at the Dragon beamline (U4B) of the NSLS (BNL, USA) in the fluorescence detection mode. The base pressure in the spectrometer chamber was better than 10^{-9} mbar. The energy resolution using a slit width of 10 μm was estimated to 0.11 eV at O K-edges.

A standard procedure was used to remove the background contribution from the pre-edge baseline of the spectra. Then the normalization for the various studied compounds was obtained by equalizing the integrated area under the high energy part of the spectra also called covalent spectra between 532 and 550 eV. All spectra at O K-edge were calibrated using the standard O 1s absorption energy of the first peak of NiO.

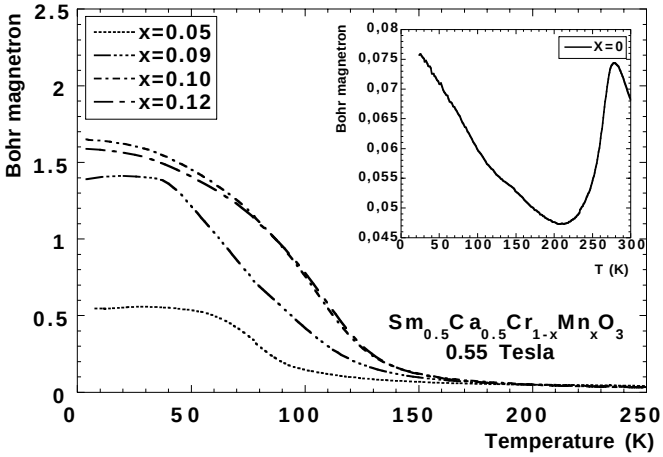

Fig. 1. Thermal variation of the magnetization of the samples $Sm_{0.5}Ca_{0.5}Mn_{1-x}Cr_xO_3$ ($0.05 \leq x \leq 0.12$) at 0.55 T.

3 Results

3.1 Physical properties

The thermal variations of the magnetization measured in a magnetic field of 0.55 T are shown in Figure 1. The ferromagnetic moment measured at low temperature (T = 5 K) increases with increasing x up to x = 0.10 and then decreases. The magnetization of the undoped compound is shown as an inset in Figure 1. As reported elsewhere [9,14], such a magnetic behavior was already observed for these doped manganites: the introduction of chromium cancels charge ordering and induces a partial spin-realignment of manganese ions due to ferromagnetic coupling.

Figure 2 shows the thermal variations of the resistance under local earth magnetic field. The curves exhibit an insulator-metal transition for $0.05 \leq x \leq 0.09$. For higher doping, a semiconducting behavior is observed. Even under weak applied magnetic field (0.55 tesla) for x = 0.10 substitution rate, no semi-conducting/metal-like transition could be observed with decreasing temperature (inset Fig. 2). The behavior of both x = 0.10 and x = 0.12 doped compounds, which remain insulating over the whole temperature range under the earth field but exhibit a ferromagnetic ordering below 100 K, was already observed for the ferromagnetic- insulators $Nd_{0.7}Ca_{0.3}MnO_3$ [15] and $Pr_{0.7}Ca_{0.3}MnO_3$ [16]. But, a transition from an insulating state to a metal-like state could be induced in the latter compounds by applying a magnetic field [17] or by exposure to X-rays or electrons beams [18] whereas the $Sm_{0.5}Ca_{0.5}Mn_{1-x}Cr_xO_3$ (x = 0.10 and x = 0.12) compounds start to exhibit a small transition only under 7 tesla. Thus, contrary to $Nd_{0.7}Ca_{0.3}MnO_3$ and $Pr_{0.7}Ca_{0.3}MnO_3$, the latter chromium doped compounds do not present a charge ordering phenomena as seen by electron microscopy.

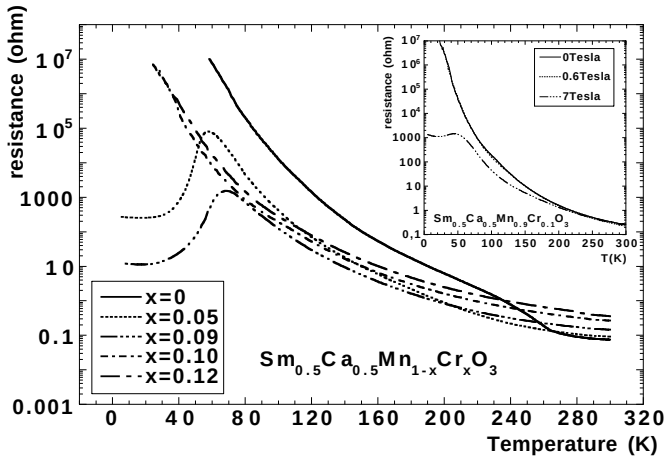

Fig. 2. Thermal variation of the resistance of the samples $Sm_{0.5}Ca_{0.5}Mn_{1-x}Cr_xO_3$ ($0.05 \leq x \leq 0.10$).

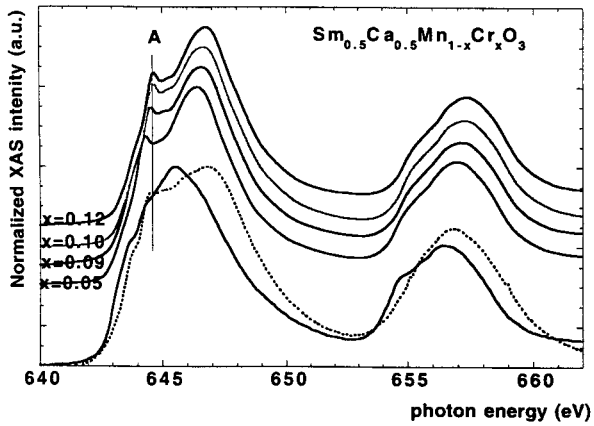

Fig. 3. XAS spectra of $Sm_{0.5}Ca_{0.5}Mn_{1-x}Cr_xO_3$ ($0.05 \leq x \leq 0.12$) at the Mn $L_{2,3}$-edge at $T = 20$ K for $H = 0.55$ T with $PrMnO_{3-\delta}$ (dot line) and $CaMnO_{3-\delta}$ (continuous line) manganese references.

3.2 Low temperature XAS study at Mn $L_{2,3}$-edges

The Mn $L_{2,3}$-edges of the $Sm_{0.5}Ca_{0.5}Mn_{1-x}Cr_xO_3$ series are shown in Figure 3. The spectra were obtained by averaging spectra recorded under 0.55 tesla with opposite helicities. The shoulder A corresponds to Mn^{4+} ($3d^3$) as previously observed [19]. A shift towards high energy by 0.3 eV is observed with increasing x. This could indicate an increasing amount of Mn^{4+} whose main absorption edge comes out at higher energy (647 eV) compared to 645 eV for Mn^{3+}. Similar shifts were already observed for $Nd_{1-x}Ca_xMnO_3$ compounds [20], for $La_{1-x}Sr_xMnO_3$ compounds [21] and for cobalt doped lanthanum manganites [22]. This result supports earlier X-ray absorption work at the Mn K-edge on cobalt, nickel or chromium doped manganites [10]. It is a new evidence that an increase of the manganese formal charge can be induced by chromium doping to keep the 'O_3' stoichiometry of the perovskite. However, this energy shift remains weak for the studied substitution rates in agreement with the maximum shift of Mn formal charge which can be estimated to +3.57 for $x = 0.12$.

3.3 Low temperature XAS study at Cr $L_{2,3}$-edges

The Cr $L_{2,3}$-edges of the $Sm_{0.5}Ca_{0.5}Mn_{1-x}Cr_xO_3$ series ($0.05 \leq x \leq 0.12$) and of Cr_2O_3 reference are shown in Figure 4. They show changes in the fine structure of both $L_{2,3}$-edges with doping. Previous studies at the Cr K-edge of the two samples with $x = 0.05$ and 0.10 showed that chromium exhibits the Cr^{3+} formal charge [10]. Since no shift towards high energy is observed in the present Cr L_3-edges, one can conclude that the observed spectral changes are not caused by a chromium formal charge change but only by crystal field changes around the probed chromium cation. This point will be addressed furthermore in the discussion.

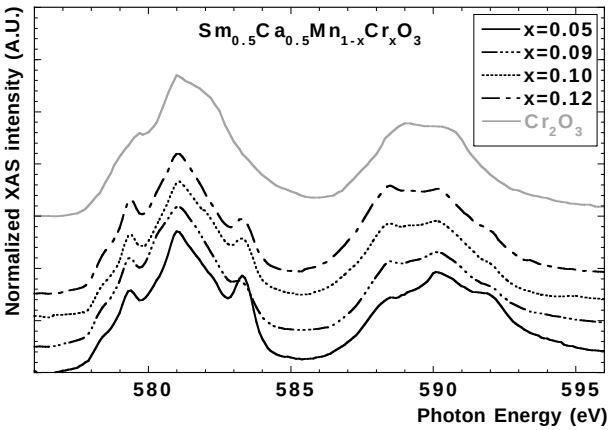

Fig. 4. XAS spectra of $Sm_{0.5}Ca_{0.5}Mn_{1-x}Cr_xO_3$ ($0.05 \leq x \leq 0.12$) at the Cr $L_{2,3}$-edge at $T = 20$ K for $H = 0.55$ T with Cr_2O_3 chromium reference [37].

3.4 Comparative low temperature XMCD study at the Cr and Mn $L_{2,3}$-edges of the $Sm_{0.5}Ca_{0.5}Mn_{1-x}Cr_xO_3$ series

The variations of the XMCD asymmetry with Cr amount are shown in Figures 5a and 5b for the Mn and Cr $L_{2,3}$-edges, respectively.

First, the qualitative but important information that can be drawn from the XMCD signals is the relative orientation of Cr and Mn magnetic subnetworks. Note that the direction of the magnetic moment carried by the probed cations aligns with the applied magnetic field. Taking the sign of the Mn $L_{2,3}$-edges as reference (Fig. 5a), one can conclude from the sign of the various XMCD spectra measured in a 0.55 T field that chromium (Fig. 5b) exhibits a magnetic moment antiparallel to the manganese magnetic moment.

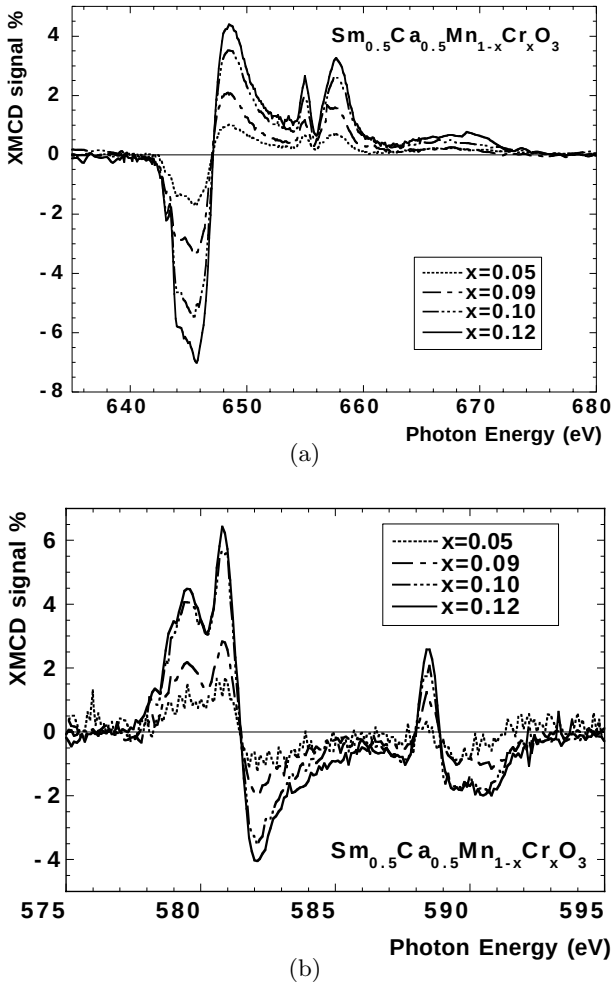

Fig. 5. XMCD signals of $Sm_{0.5}Ca_{0.5}Mn_{1-x}Cr_xO_3$ ($0.05 \leq x \leq 0.12$) at $T = 20$ K for $H = 0.55$ T (a) Mn $L_{2,3}$-edge; (b) Cr $L_{2,3}$-edge.

From a quantitative point of view, by applying sum rules [23], one should be able to estimate the operators of the orbital magnetic moment $\langle L_z \rangle$ and the operators of the spin magnetic moment $\langle S_z \rangle$ for each probed element and edge. In the case of manganese and chromium oxides, the spin-orbit splitting of the core hole is not large enough to prevent a mixing of the J contributions to the L_3- and L_2-edges [24] such that, an error of the determination up to 200% of $\langle S_z \rangle$ has been shown by the multiplet calculations [25]. Thus, one can only calculate an estimation of the orbital magnetic moment which corresponds to a quenched orbital contribution as expected in the case of the transition metal [19].

The increase of both magnetic moments carried by the Mn and Cr cations with increasing doping ratio is clearly deduced from the increase of the SXMCD asymmetries. Thus, an introduction of chromium causes spin-realignment of a part of the manganese cations to create a ferromagnetic manganese sublattice antiparallel to a ferromagnetic chromium sublattice. In contrast to magnetic multilayers systems [26], it is difficult to determine an average magnetic moment on the perovskite B site by comparison with a reference manganite because of the intrinsic properties of the manganese-oxygen bonds [27]. In manganese oxides, the magnetization depends on the Mn-O distance and on the O-Mn-O angle which is linked to the mean A-site cation radius $\langle r_a \rangle$ which induces a reduction of the O-Mn-O angle and on the filling of the Mn($3d$)-O($2p$) molecular orbitals *i.e.* on the Mn^{4+}/Mn^{3+} ratio. Nevertheless, one can consider an average magnetic moment on the B site estimated by the sum of the weighted asymmetries found at Cr-and Mn $L_{2,3}$-edge (Tab. 1): these asymmetries show a rough agreement with the variations of the total magnetization. The two antiparallel manganese and chromium sublattices compensate each other and, for a critical Cr doping ratio, the decrease of total magnetic moment starts to be observable on the magnetization curve (Fig. 1).

At least, no change in the fine structure of the XMCD signal at Mn and Cr $L_{2,3}$-edges was observed with increasing doping amount. Cr $L_{2,3}$-edge XMCD spectra are compatible with atomic calculations performed by van der Laan [28] for Cr^{3+} in an octahedral symmetry which confirmed once again the Cr^{3+} formal charge independent of the doping ratio as observed from XAS measurements at Cr $L_{2,3}$- and K-edges.

3.5 Low temperature XAS and XMCD studies at O K-edge

The O K-edges of the $Sm_{0.5}Ca_{0.5}Mn_{1-x}Cr_xO_3$ series ($0 \leq x \leq 0.12$) and of Cr_2O_3 taken from [29] are shown in Figures 6a and 6b. The pre-edge structure is linked for transition metal oxides to the metal $3d$ through hybridization with the O $2p$ orbitals as shown previously by de Groot and coworkers [30]. One observes a smoothing of the A' structure by doping of the perovskite B site with chromium. Figures 6a, b and c illustrates chromium doping effects on the pre-edge structure. More precisely, chromium doping induces a shift towards high energy of the pre-edge structure (< 534.5 eV) (Figs. 6b, c) and a reduction of the intensity pre-edge A (Fig. 6b).

As noticed above, an increase of the manganese formal charge is induced by chromium doping to keep the 'O_3' stoichiometry of the perovskite. This manganese formal charge increase is linked to a shift towards high energy at Mn $L_{2,3}$-edge (Fig. 3) and should induce a shift towards low energy at O K-edge as it observed on other manganites series [31].

But, taking into account both manganese and chromium hybridization with the probed O $2p$ orbitals, one can easily understand the observed structure change induced by doping of the perovskite B site with chromium. The introduction of chromium decreases the A structure intensity which is more or less compensated by an increase of the area under the A' structure (Fig. 6b). Upon chromium doping, the A' structure results from an admixture of the e_g spin- down Mn^{3+} and Mn^{4+} subbands with

Table 1. XMCD asymmetries at chromium and manganese $L_{2,3}$-edges and comparison between the weighted asymmetries on perovskite B site and the magnetization recorded on the same experimental condition (T = 20 K; H = 0.55 T) in the $Sm_{0.5}Ca_{0.5}Mn_{1-x}$ Cr_xO_3 series.

$Sm_{0.5}Ca_{0.5}Mn_{1-x}Cr_xO_3$	Cr XMCD at 580.8 eV %	Mn XMCD at 645.6 eV %	Weighted asymmetries on perovskite B site %	Magnetization μ_B
$x = 0.05$	+ 1.5	−1.4	−1.25	0.55
$x = 0.09$	+ 2.8	−3.0	−2.48	1.40
$x = 0.10$	+ 5.7	−4.1	−3.12	1.62
$x = 0.12$	+ 6.4	−4.7	−3.37	1.56

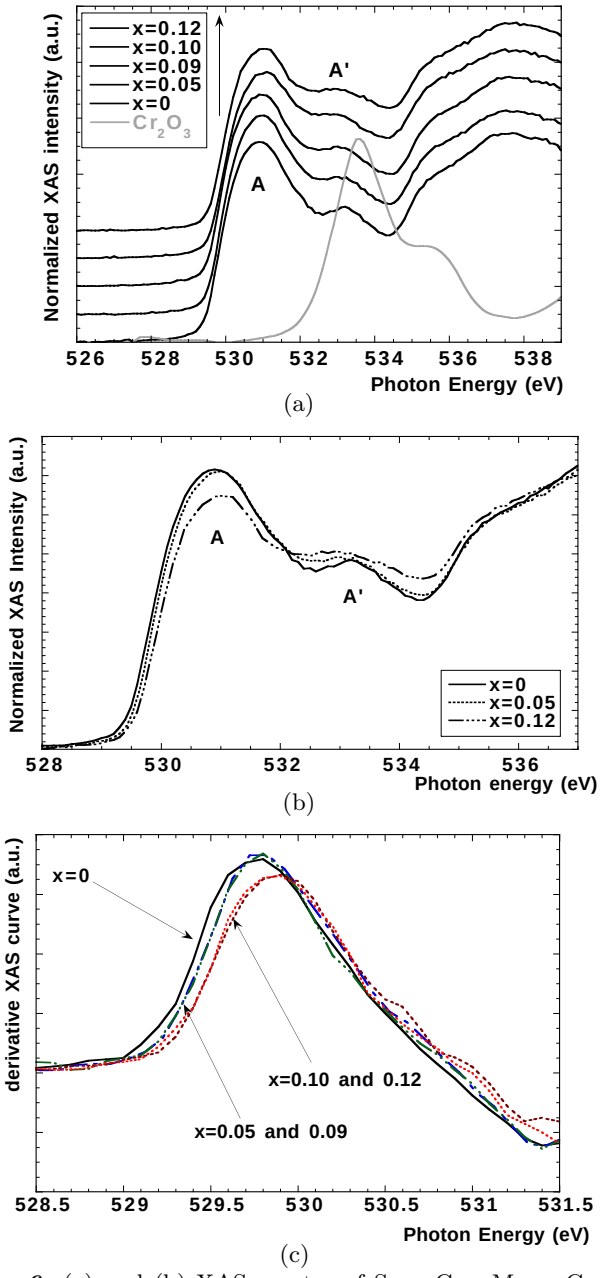

Fig. 6. (a) and (b) XAS spectra of $Sm_{0.5}Ca_{0.5}Mn_{1-x}Cr_xO_3$ ($0.00 \leq x \leq 0.12$) at the O K-edge at T = 20 K with Cr_2O_3 chromium reference [29]; (c) derivative XAS spectra of $Sm_{0.5}Ca_{0.5}Mn_{1-x}Cr_xO_3$ ($0.00 \leq x \leq 0.12$) on the same experimental conditions.

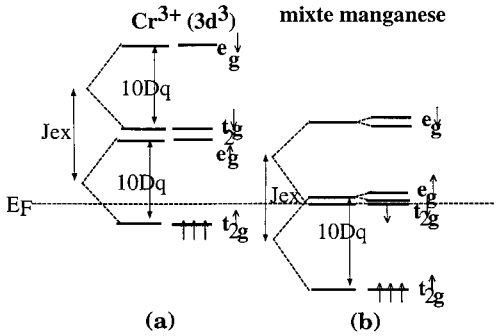

Fig. 7. (a) Schematic energy level diagram of molecular orbitals for Cr(III); (b) mixte valent Mn(III)/Mn(IV) and Cr(III). The respective values of the exchange interaction parameter J_{exc} and of the crystal field strength 10 Dq were estimated previously by Kurata [32] from cluster calculation.

e_g spin-up and t_{2g} spin down Cr^{3+} subbands as depicted in the energy level diagram (Fig. 7). Note that the first empty molecular manganese band above the Fermi level (Fig. 7b) is attributed to a minority t_{2g} molecular band mixed with a majority e_g molecular band in agreement with the O-K XMCD measurements on $Sm_{0.5}Ca_{0.5}Mn_{0.9}Cr_{0.1}O_3$ compound which shows an XMCD asymmetry of about −0.8% (Fig. 8). The Figure 7b scheme is also based on the relative interplay of the crystal field effect noted as 10 D_q and the exchange energy noted as J_{ex} which splits the t_{2g} and e_g orbitals and the spin up and down levels as [32] and, takes into account weakly distorted MnO_6 octahedra in Cr-doped compounds as observed by neutron diffraction [33].

Let us now consider the O-K XMCD measurements of $Sm_{0.5}Ca_{0.5}Mn_{0.9}Cr_{0.1}O_3$ compound. First, taking into account the negative SXMCD signal at the O K-edge (Fig. 8) compared with the negative SXMCD signal at the Mn $L_{2,3}$-edges, which one concluded from that the observed orbital magnetic moment on oxygen is parallel to the manganese orbital magnetic moment. Note that, as an antiparallel magnetic moment ordering between samarium and manganese sublattices was previously shown in the same compounds [14], at low temperature, an overall ferrimagnetic ordering is observed in the $Sm_{0.5}Ca_{0.5}Mn_{0.9}Cr_{0.1}O_3$ compound.

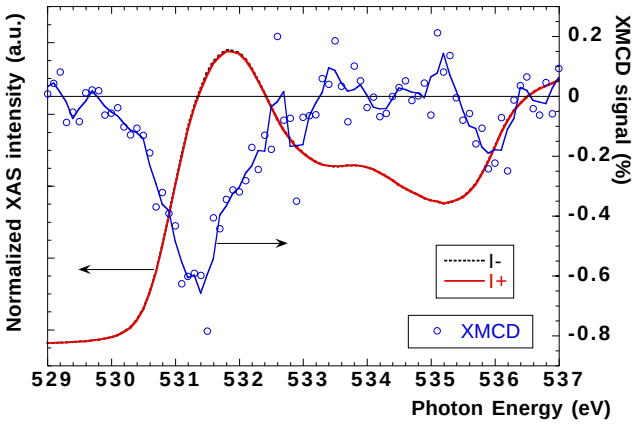

Fig. 8. O K-edge XMCD signals of $Sm_{0.5}Ca_{0.5}Mn_{0.9}Cr_{0.1}O_3$ at $T = 20$ K for $H = 0.55$ T.

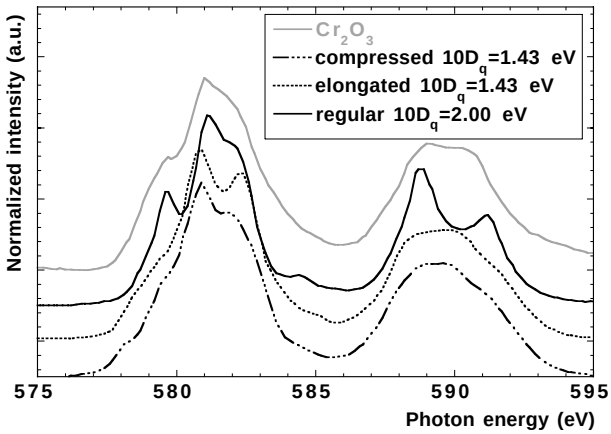

Fig. 9. Multiplet simulation of regular, elongated and compressed octahedral Cr^{3+} from de Groot and observed Cr $L_{2,3}$-edges for Cr_2O_3 at room temperature [37].

Moreover, as observed before [6], O K-edge show a single peak structure which is usually observed for semiconducting samples. The XMCD asymmetry is small compared with values published by Pellegrin [34] (-1.6% for $La_{1-x}Sr_xMnO_3$ ($x = 0.18$ and $x = 0.4$) and for similar temperatures, applied magnetic field and light circular polarization). This could be due to the difference in magnetization between the Sr-substituted lanthanum manganites [35] and Cr-doped samarium manganites (Fig. 1). It is likely that such a small effect corresponds to a dipolar induced polarization of the O valence electrons by the magnetic moment born by the Mn network. This observation is compatible with the idea that doped holes present an O ($2p$) character with majority t_{2g} spin-down polarization mixed with e_g spin-up, in agreement with crystal field and band structure calculations [36].

4 Discussion

This soft XAS and XMCD study of some Cr doped rare earth CMR manganites was undertaken to investigate how such small Cr doping could cancel charge ordering and induce CMR properties in a specific doping range ($0.05 \leq x \leq 0.09$). Two kinds of information can be drawn from the spectra: the local distortions from the XANES analysis and the magnetic ordering of Cr and Mn cations from XMCD.

4.1 XANES analysis

Here, we will consider the Cr $L_{2,3}$-edges (Fig. 4) where strong changes can be observed at both edges with the Cr doping whereas no significant changes in the fine structure can be seen at Mn $L_{2,3}$-edges (Fig. 3). First TT-multiplets simulations of the $L_{2,3}$-edges of chromium realized by de Groot within a simple framework of octahedral coordination around Cr^{3+} and tetragonal distortion are shown in Figure 9. These first TT-multiplets calculations did take into account neither the real unknown distortion of the CrO_6 octahedra nor the charge transfer contributions ($3d^4\underline{L}$ in the case of Cr^{3+} cations) but are simulations for regular, elongated and compressed octahedra using indicated crystal field and distortion values. These simulations are compared to the experimental $L_{2,3}$-edge of Cr_2O_3 [37].

The spectra of the slightly doped manganites appear different from the regular octahedron case and let us assume that the Cr octahedra must be strongly distorted. Conversely the similarity at L_2-edge between the Cr_2O_3 spectrum and the samarium manganite with the highest doping rate ($x = 0.12$) allows to assume that the CrO_6 octahedra distortion are comparable. Both are also close to the regular octahedron simulation. But, for all the manganites, the main difference arises from the presence of two shoulders at 583 and 592 eV on the high energy sides of L_3 and L_2 peaks respectively. These extra peaks could be generated by the charge transfer configuration $|3d^4\underline{L}\rangle$. Thus one is led to conclude that simple TT-multiplet simulations can not fit properly the Cr substituted samarium manganites at Cr $L_{2,3}$-edges. More accurate calculations must be realized taking into account the real symmetry around Cr cations and the charge transfer configuration.

Nevertheless, what is also clearly visible in the manganite spectra is the strong variation in intensity of the so-called charge transfer lines at 583 and 592 eV. This result is a clear indication of a variation of the Cr-O bond covalency with doping ratio and consequently of a variation of exchange interactions with the Mn network. Changes observed at O-K edge spectra provide same kind of information. They show also that the contribution of the charge transfer configurations to the spectral density is higher for low chromium doping compounds than for the highest one.

Anyway, Cr ($3d$) orbitals overlap with the O ($2p$) ones and would participate at low chromium doping to the conduction band allowing the transition to the metallic state

to be realized. Question is now what is the main force which drive the resistance transition.

Since Cr^{3+} ($3d^3$) is not a Jahn-Teller cation, CrO_6 octahedra would not accept in their direct neighborhood the strong distortions created by the charge ordering mechanism. The transition to the metallic state is induced by a reduction of the charge ordering which favors carrier delocalization, with chromium ratio increase. The total disappearance of the charge ordering phenomena [11] occurs for $x = 0.05$ which present an insulator-metal transition. Therefore, in the case of the $Sm_{0.5}Ca_{0.5}Mn_{1-x}Cr_xO_3$ series at intermediate doping rates, the main force driving the resistance transition should be based on the manganese ferromagnetic ordering following the double-exchange model.

4.2 Model of magnetic ordering

The SXMCD analysis may also allow to understand what happens for Cr doped manganites. Form Figures 5a and b, the ferromagnetism of the manganese network itself is induced by the negative super exchange interaction Cr^{3+}-O^{2-}-Mn^{4+} and by the positive double exchange interaction Mn^{4+}-O^{2-}-Mn^{3+} as predicted by Joncker [38]. Then, a simple phenomenological model allows us to understand how the introduction of small doping amounts of Cr can induce spin alignment on the Mn sublattice in order to create a ferromagnetic sublattice antiparallel to the Cr^{3+} cations as observed by XMCD.

In the case of low doping amounts, spin alignment on the Mn sublattice occurs in small domains around the Cr sites. Upon increasing doping the number of manganese atoms involved in ferromagnetic ordering increase in agreement with the increase of the total magnetization. The system is then electronically phase-separated into a mixture of insulating regions originating from a high concentration of negative interactions Mn^{4+}-O^{2-}-Mn^{4+}, Mn^{3+}-O^{2-}-Mn^{3+} or Cr^{3+}-O^{2-}-Cr^{3+}, and ferromagnetic/metallic domains around chromium cations originating from positive interactions Cr^{3+}-O^{2-}-Mn^{4+} and Mn^{4+}-O^{2-}-Mn^{3+}.

As in the case of the highest doping ratio, chromium doping induces a decrease of Mn^{3+}/Mn^{4+} ratio [10], the negative super-exchange interactions Mn^{4+}-O^{2-}-Mn^{4+} and Cr^{3+}-O^{2-}-Cr^{3+} become stronger than positive the double exchange interactions Cr^{3+}-O^{2-}-Mn^{4+} and Mn^{4+}-O^{2-}-Mn^{3+}. More, as emphasized above, for x larger than 0.1, the Cr^{3+} orbitals contribute less to the band conduction thus preventing any phase transition to a metallic state.

5 Conclusion

In this work, we have presented soft XAS and XMCD measurements at low temperature ($T = 20$ K) of Cr doped samarium manganites with the general formula $Sm_{0.5}Ca_{0.5}Mn_{1-x}Cr_xO_3$ ($0.05 \leq x \leq 0.12$). This series of compounds was chosen because it exhibits a wide variety of structural and physical properties going from the insulating charge ordered behavior for the parent compound $Sm_{0.5}Ca_{0.5}MnO_3$ to CMR properties for $0.05 \leq x \leq 0.09$ and shifting to a ferromagnetic-insulator upon increasing x.

XAS at O-K and Cr $L_{2,3}$-edges showed clear changes in the spectra upon increasing x which have been interpreted as a variation of the covalence of the Cr-O bond. XMCD at Cr and Mn $L_{2,3}$-edges showed that Cr magnetic moments align anti-parallel to the Mn magnetic moments. Such a result is quite new and show that soft XMCD is now a unique probe to investigate the magnetic interactions even at low element concentrations.

A simple phenomenological model which supports an electronically phase-separated system, is proposed based on a simple analysis of XANES and XMCD spectra. It allows to understand the nature of magnetic interactions in the doped manganites. However, accurate TT-multiplets simulations of Cr and Mn $L_{2,3}$-edges will be necessary to investigate in more details the local structural distortions which are the driving forces of the physical transitions.

We are grateful to J.H. Park of the NSLS in Brookhaven for his help and advices during the X-ray absorption experiment and to F.M.F. de Groot for his first TT-multiplets simulations.

References

1. R.M. Kuster, J. Singleton, D.A. Keon, R.M. Greedy, W. Hayes, Physica B **155**, 362 (1989); R. Von Hemmolt, J. Wecker, B. Holzapfel, L. Schultz, K. Samwer, Phys. Rev. Lett. **71**, 2331 (1993); S. Jin, T.H. Tiefel, M. Mc Cormack, R.A. Fastnacht, R. Ramesh, L.H. Chen, Science **264**, 413 (1994).
2. C. Zener, Phys. Rev. **82**, 403 (1951); P.W. Anderson, H. Hasegawa, Phys. Rev. **100**, 975 (1955); P.G. de Gennes, Phys. Rev. **118**, 141 (1960).
3. A.J. Millis, P.B. Litlewood, B.I. Shraiman, Phys. Rev. Lett. **74**, 5144 (1995) and A.J. Millis, B.I. Shraiman, R. Mueller, Phys. Rev. Lett. **77**, 175 (1996).
4. V. Caignaert, E. Suard, A. Maignan, Ch. Simon, B. Raveau, J. Magn. Magn. Mater. **153**, L260 (1996); J.L. Garcia-Munoz, M. Suaaidi, J. Fontcuberta, J. Rodriguez-Carvajal, Phys. Rev. B **55**, 34 (1997); P. Dai, J. Zhang, H.A. Mook, S.H. Liou, P.A. Dowben, E.W. Plummer, Phys. Rev. B **54**, R3694 (1996).
5. C. Meneghini, R. Cimino, S. Pascarelli, S. Mobilio, C. Raghu, D.D. Sarma, Phys. Rev. B **56**, 3520 (1997); C.H. Booth, F. Bridges, G.H. Kwei, J.M. Lawrence, A.L. Cornelius, J.J. Neumeier, Phys. Rev. lett. **80**, 853 (1998).
6. O. Toulemonde, F. Millange, F. Studer, B. Raveau, J.-H. Park, C.-T. Chen, J. Phys. Condens. Matter **11**, 109 (1999).
7. F. Studer, O. Toulemonde, V. Caignaert, P. Srivastava, J. Goedkoop, N. Brookes, J. Phys. IV France **7**, C2-529 (1997).

8. A. Moreo, S. Yunoki, E. Dagotto, Science **283**, 2034 (1999); M. Uehara, S. Mori, C.H. Chen, S.W. Cheong, Nature **399**, 560 (1999); J. Baszynski, J. Kovac, A. Kowalczyk, J. Magn. Magn. Matter **195**, 93 (1999); R. Mahendiran, *et al.*, Solid State Com. **114**, 429 (2000); Y. Moritomo, A. Machida, S. Mori, N. Yamamoto, A. Nakamura, Phys. Rev. B **60**, 9220 (1999).
9. B. Raveau, A. Maignan, C. Martin, J. Solid State Chem. **130**, 162 (1997); A. Maignan, F. Damay, C. Martin, B. Raveau, Mater. Res. Bull. **32**, 965 (1997); A. Barnabe, A. Maignan, M. Hervieu, F. Damay, C. Martin, B. Raveau, Appl. Phys. Lett. **71**, 3907 (1998).
10. O. Toulemonde, F. Studer, A. Barnabé, A. Maignan, C. Martin, B. Raveau, Eur. Phys. J. B **4**, 159 (1998).
11. A. Barnabé, M. Hervieu, C. Martin, A. Maignan, B. Raveau, J. Mater. Chem. **8**, 1405 (1998).
12. M. Drescher, G. Schnell, U. Kleineberg, H.J. Stock, N. Muller, U. Heinzmann, N.B. Brookes, Rev. Sci. Instrum. **68**, 1939 (1996).
13. C.T. Chen, Y.U. Idzerda, H-J. Lin, N.V. Smith, G. Meigs, E. Chaban, G.H. Ho, E. Pellegrin, F. Sette, Phys. Rev. Lett. **75**, 152 (1995).
14. O. Toulemonde, F. Studer, A. Barnabé, B. Raveau, J.B. Goedkoop, J. Applied Phys. **86**, 2616 (1999).
15. F. Millange, V. Caignaert, G. Mater, E. Suard, B. Raveau, J. Solid State Chem. **127**, 131 (1996).
16. Z. Jirak, S. Krupicka, Z. Simsa, M. Dlouha, S. Vratislav, J. Magn. Magn. Mater. **53**, 153 (1985).
17. Y. Tomioka, A. Asamitsu, Y. Moritomo, Y. Tokura, J. Phys. Soc. Jpn **64**, 3626 (1995).
18. D.E. Cox, P.G. Radaelli, M. Marezio, S.W. Cheong, Phys. Rev. B **57**, 3305 (1998); M. Hervieu, A. Barnabé, C. Martin, A. Maignan, B. Raveau, Phys. Rev. B **60**, R726 (1999); V. Kiryukine, D. Casa, J.P. Hill, B. Keimer, A. Vigliante, Y. Tomioka, Y. Tokura, Nature **386**, 813 (1997); K. Miyano, T. Tanaka, Y. Tomioka, Y. Tokura, Phys. Rev. Lett. **78**, 4257 (1997).
19. O. Toulemonde, F. Studer, A. Lobet, L. Ranno, A. Maignan, E. Pollert, M. Nevriva, E. Pellegrin, N.B. Brooks, J. Goedkoop, J. Magn. Magn. Mater. **190**, 307 (1998).
20. R.S. Liu, J.B. Wu, C.Y. Chang, J.G. Lin, C.Y. Huang, J.M. Chen, R.G. Liu, J. Solid State Chem. **125**, 112 (1996).
21. M. Abbate, F.M.F. de Groot, J.C. Fuggle, A. Fujimori, O. Strebel, F. Lopez, M. Domke, G. Kaindl, G.A. Sawatsky, M. Takeda, H. Eisaki, S. Uchibara, Phys. Rev. B **46**, 4511 (1992).
22. J.H. Park, S.W. Cheong, C.T. Chen, Phys. Rev. B **55**, 11072 (1997).
23. B.T. Thole *et al.*, Phys. Rev. Lett. **68**, 1943 (1992); P. Carra *et al.*, Phys. Rev. Lett. **70**, 694 (1993).
24. Y. Teramura, A. Tanaka, T. Jo, J. Phys. Soc. Jpn **65**, 1053 (1996).
25. E. Pellegrin (private communication).
26. Y.U. Idzerda, L.H. Tjeng, H.J. Lin, C.J. Guttierrez, G. Meigs, C.T. Chen, Phys. Rev. B **48**, 4144 (1993); S. Andrieu, E. Foy, H. Fischer, M. Alnot, F. Chevrier, G. Krill, M. Piecuch, Phys. Rev. B **58**, 8210 (1998); M.A. Tomaz, W.J. Antel Jr, W.L. O'Brien, G.R. Harp, Phys. Rev. B **55**, 3716 (1997).
27. J.L. Garcia-Munoz, J. Fontcuberta, B. Martinez, A. Seffar, S. Pignol, X. Obradors, Phys. Rev. B **55**, R668 (1997).
28. G. van der Laan, B.T. Thole, Phys. Rev. B **43**, 13401 (1991).
29. O.L. Krivanek, J.H. Paterson, Ultramicroscopy **32**, 313 (1990).
30. F.M.F. de Groot, M. Grioni, J.C. Fuggle, J. Ghijsen, G.A. Sawatzky, H. Petersen, Phys. Rev. B **40**, 5715 (1989).
31. J.H. Park, C.T. Chen, S.-W. Cheong, W. Bao, G. Meigs, V. Chakarian, Y.U. Idzerda, Phys. Rev. Lett. **76**, 4215 (1996); F.M.F. de Groot, Ph.D. Thesis University of Groningen, (1991); D.D. Sarma, O. Rader, T. Kachel, A. Chainani, M. Mathew, K. Holldack, W. Gudat, W. Eberhardt, Phys. Rev. B **49**, 14238 (1994).
32. H. Kurata, C. Colliex, Phys. Rev. B **48**, 2101 (1993).
33. F. Damay, C. Martin, A. Maignan, M. Hervieu, B. Raveau, F. Bourée, G. André, Appl. Phys. Lett. **73**, 3772 (1998).
34. E. Pellegrin, L.H. Tjeng, F.M.F. de Groot, R. Hesper, C.F.J. Flipse, J.D. O'Mahony, Y. Moritomo, Y. Tokura, C.T. Chen, G.A. Sawatzky, J. Phys. IV France **7**, C2-405 (1997).
35. A. Urushibara, Y. Moritomo, T. Arima, A. Asamitsu, G. Kido, Y. Tokura, Phys. Rev. B **51**, 14103 (1995).
36. W.E. Pickett, D.J. Singh, Phys. Rev. B **53**, 1146 (1996); S. Satpathy, Z.S. Popovic, F.R. Vukajlovic, Phys. Rev. Lett. **76**, 960 (1996); Z. Yang, L. Ye, X. Xie, Phys. Rev. B **59**, 7051 (1999); S.F. Matar, F. Studer, B. Siberchicot, M.A. Subramaniam, G. Demazeau, J. Etourneau, Eur. Phys. J. AP **4**, 143 (1998).
37. J.H. Park (private communication).
38. G.H. Joncker, Physica **22**, 707 (1956).